

See discussions, stats, and author profiles for this publication at: <https://www.researchgate.net/publication/255174362>

First Observation of Photons Carrying Orbital Angular Momentum in Undulator Radiation

Article in *Physical Review Letters* · July 2013

DOI: 10.1103/PhysRevLett.111.034801 · Source: PubMed

CITATIONS

26

READS

137

6 authors, including:



[Karsten Holldack](#)

Helmholtz-Zentrum Berlin

161 PUBLICATIONS 1,872 CITATIONS

[SEE PROFILE](#)



[Peter Kuske](#)

Helmholtz-Zentrum Berlin

101 PUBLICATIONS 1,100 CITATIONS

[SEE PROFILE](#)



[Roland Mueller](#)

Helmholtz-Zentrum Berlin

28 PUBLICATIONS 67 CITATIONS

[SEE PROFILE](#)



[Michael Scheer](#)

Helmholtz-Zentrum Berlin

59 PUBLICATIONS 461 CITATIONS

[SEE PROFILE](#)

All content following this page was uploaded by [Karsten Holldack](#) on 10 April 2015.

The user has requested enhancement of the downloaded file. All in-text references [underlined in blue](#) are added to the original document and are linked to publications on ResearchGate, letting you access and read them immediately.

First Observation of Photons Carrying Orbital Angular Momentum in Undulator Radiation

J. Bahr¹dt, K. Holldack, P. Kuske, R. Müller, M. Scheer, and P. Schmid

Helmholtz-Zentrum Berlin, Albert-Einstein-Straße 15, 12489 Berlin, Germany

(Received 26 February 2013; published 15 July 2013)

Photon beams of 99 eV energy carrying orbital angular momentum (OAM) have been observed in the 2nd harmonic off-axis radiation of a helical undulator at the 3rd generation synchrotron radiation light source BESSY II. For detection, the OAM carrying photon beam was superimposed with a reference beam without OAM. The interference pattern, a spiral intensity distribution, was recorded in a plane perpendicular to the propagation direction. The orientation of the observed spiral structure is related to the helicity of the undulator radiation. Excellent agreement between measurements and simulations has been found.

DOI: [10.1103/PhysRevLett.111.034801](https://doi.org/10.1103/PhysRevLett.111.034801)

PACS numbers: 41.60.Ap, 41.60.Cr

Introduction.—For an axially symmetric geometry the solution of the Helmholtz equation in paraxial approximation can be expanded in Laguerre-Gaussian (LG) polynomials. In 1992, Allen *et al.* demonstrated analytically that beams consisting of an i th LG mode with a cork-screw-like phase distribution and an annular intensity carry an orbital angular momentum of $l\hbar$ [1] per photon. Since then, various experiments using OAM-photons were performed in the visible and in the infrared regime [2,3]. OAM photons were utilized for the micromanipulation of small particles in optical tweezers [4] or for channel multiplexing in telecommunication [5]. Also, OAMs lead to other selection rules for electronic transitions, e.g., quadrupole transitions, forbidden for Hermite Gaussian (HG) beams are allowed if spin and orbital angular momentum add up to two [6]. So-called OAM dichroism spectroscopy is feasible if the beam size is of the same magnitude as the sample region [6]. Already today, focus sizes well below 20 nm are achievable with high quality zone plates as described in [7,8]. However, a widespread use of OAM beams is hampered by the difficulties to generate such beams.

The first transformation of the more common HG beams into LG beams has been performed with cylindrical lenses [9]. Today, sophisticated computer-controlled spatial light modulators are used to generate forked holographic patterns which transform HG modes into LG modes in the ± 1 st diffraction order of the forked hologram [10].

Singular photon beams—another name for OAM beams emphasizing the phase singularities—have been obtained in the x-ray regime as well. So far, they were produced either with a circular phase plate [11] or with a simple rectangular aperture [12] from transversal coherent spherical waves. Both experiments were performed at 3rd generation storage rings (APS and SPRING-8, respectively). The light generated in these experiments was a mixture of many modes and the energy tunability was limited.

Various schemes of singular photon beam production in free electron lasers (FELs) based on helical undulators have been proposed. One method uses a CO₂ seed laser,

resonant to the 2nd harmonic of a helical undulator, which is superimposed to the electron bunch while passing the undulator [13]. The FEL mechanism in the presence of the CO₂ laser field gradient forces the electrons on a cork-screw-like charge distribution with a period of half the resonance wavelength. Only recently, a spiral or helical bunching in the 2nd harmonic has been observed [14]. Helical bunching on the 1st FEL harmonic can be achieved in a harmonic generation scheme where a seed laser is superimposed to the electron beam in a helical modulator. A chicane converts this energy modulation into a helical bunching which is transferred to the FEL radiator [15]. At short wavelengths, the required strong seed lasers are not available and alternative schemes are proposed. The echo enabled harmonic generation (EEHG) seeding scheme is predicted to generate intense x-ray OAM beams at the FEL fundamental [16].

A direct and efficient method to generate Laguerre-Gaussian beams of high mode purity in accelerator based synchrotron radiation light facilities was theoretically predicted in 2007 [17,18]. A relativistic particle passing through a helical undulator is supposed to produce Laguerre-Gaussian modes in the off-axis radiation of the 2nd undulator harmonic. Here, we report on the first experimental proof of existence of these OAM modes.

Theory.—Higher harmonic photon beams of helical undulators carry an orbital angular momentum of $\pm(n-1)\hbar$ as described in [17], where n is the harmonic number. The OAM sign depends on the helicity of the 1st undulator harmonic. For these cases, the on-axis intensity is zero (annular beam) and the phase on a circle in a plane perpendicular to the photon beam varies with $(n-1)\varphi$, where φ is the azimuthal angle. Figure 1 shows the phase characteristics of OAM carrying beams and beams without OAM photons. OAM photons exist in a region of the parameter space where helical undulators usually are not operated because the brightness of helical undulators is reduced at higher harmonics, though the flux is still rather high.

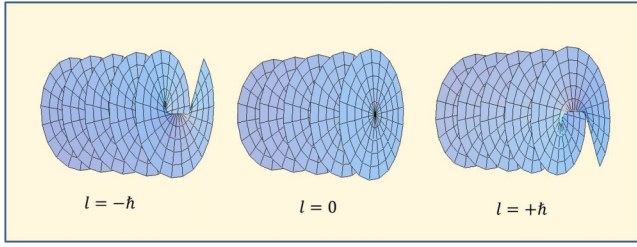


FIG. 1 (color online). Surfaces of equal phase for beams with various orbital angular momenta.

The intensity distribution of a singular photon beam does not exhibit the peculiar feature of a cork-screw-like phase distribution. Without a wave front sensor, solely relying on pure intensity measurements, the observation of photons carrying orbital angular momentum is difficult. An azimuthal intensity variation may be a hint [18] but the modulation is smeared out by electron beam emittance and photon beam line effects. A superior method is an interference experiment which utilizes the corkscrew-like phase distribution. The photon beam carrying OAMs is superimposed on a reference beam without OAM photons (or with OAM of another quantum number) monitoring the interference fringes in the intensity distribution perpendicular to the propagation direction.

Experimental setup.—The experiment was carried out at the 3rd generation electron storage ring BESSY II. The layout of the experimental setup is depicted in Fig. 2. The double undulator UE-56 [19] was used for the generation of the two light beams, the singular photon beam and the reference beam. The UE-56 double undulator consists of two APPLE II type modules [20]. Each module can be tuned individually for photon energy and polarization. The 1st undulator (upstream) was tuned to pure helical mode and a photon energy of 49.5 eV in the 1st harmonic. The reference undulator (downstream) was tuned to 99 eV and horizontal linear polarization. Other polarization states can be used for reference, as well, including circular polarization with zero or finite topological charge, as long as the

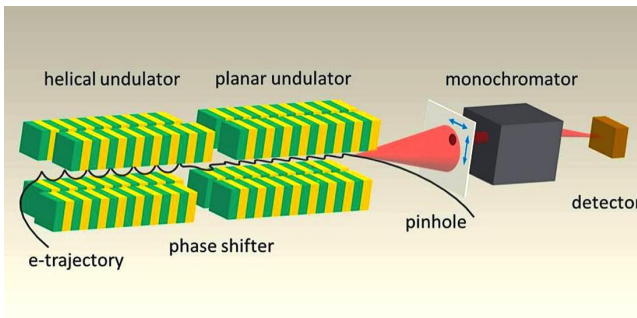


FIG. 2 (color online). Setup of the experiment with two undulators and a phase shifter in between (not shown), a movable pinhole in front of the monochromator and the detector behind the refocusing optics.

topological charges of the two beams are different. A permanent magnet phase shifter consisting of eight rotatable magnets between the two undulators [19] permits the realization of an additional phase shift between the two light beams. A monochromator behind the double undulator [21] selects a specific wavelength and narrows the bandwidth while elongating the two wave packages. Thus, the overlap of the two originally separated light beams happens only behind the monochromator (the arrangement is similar to the crossed undulator as proposed independently by Nikitin [22] and Kim [23]). The monochromator resolution was 2500, providing a longitudinal overlap of >98%. Small fractions of the interfering light beams are cut out with a $\phi 100 \mu\text{m}$ pinhole upstream of the first optical element and measured with a $\phi 4 \text{ mm}$ GaAsP diode downstream of the monochromator behind the exit slit and refocusing chamber. The transverse intensity distribution of the interfering beams was measured by so-called “pin-hole maps” where the pinhole is moved in the transverse plane while monitoring the diode signal.

The basic pattern of the expected intensity distribution can be evaluated from a simple model where the OAM carrying beam and the linearly polarized beam are both described by point sources (far field approximation). Only the horizontal electric field components interfere whereas the vertical component of the helical undulator contributes to an independent intensity background. The horizontal field amplitudes of both beams, A and B , are described by the real expressions

$$A(r, \varphi) = \frac{a(r)}{L+d} \cos\left(\frac{\pi d}{\gamma^2 \lambda} + \frac{\pi}{(L+d)\lambda} r^2 \pm (n-1)\varphi + \frac{2\pi L}{\lambda} - \omega t\right), \quad (1)$$

$$B(r, \varphi) = \frac{b(r)}{L} \cos\left(\frac{\pi}{L\lambda} r^2 + \frac{2\pi L}{\lambda} - \omega t\right) \quad (2)$$

with L = distance between the linear undulator and plane of the pinhole (12 237 mm), d = distance between the helical and linear undulator (2126 mm), r = transverse distance to beam axis, λ = photon wavelength, ω = detection frequency, t = time, $a(r)$ and $b(r)$ radial part of the field amplitudes and γ = Lorentz factor of the relativistic electrons.

The intensity distribution of the horizontal field components is evaluated from Eqs. (1) and (2) via

$$I(r, \varphi) = \frac{\omega}{2\pi} \int_0^{2\pi} (A+B)^2 dt \quad (3)$$

leading to

$$I(r, \varphi) = \frac{a^2}{2(L+d)^2} + \frac{b^2}{2L^2} + \frac{ab}{L(L+d)} \times \cos\left(\frac{\pi d}{\gamma^2 \lambda} - \frac{\pi d}{L^2 \lambda} r^2 \pm (n-1)\varphi\right). \quad (4)$$

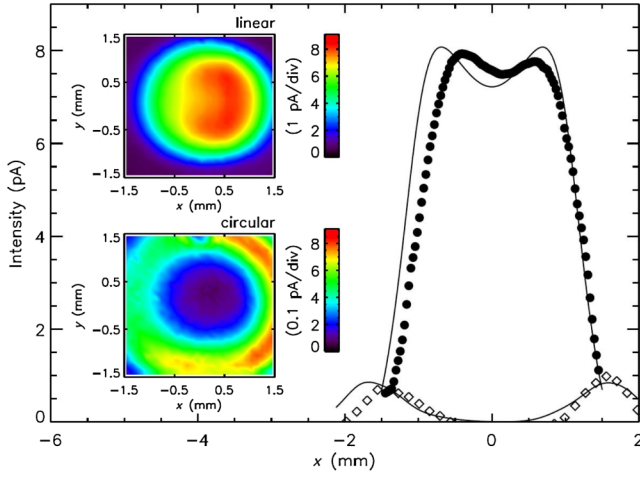


FIG. 3 (color online). Measured (symbols) and simulated (solid lines) intensity cuts of the individual undulators: vertical cuts of the linear undulator (dots and solid line) and diagonal cuts of the helical undulator (diamonds and solid line) are plotted. The unused undulator is set to a magnetic gap of 100 mm. Inset: Measured color-coded intensity profiles from the linear (upper) and the helical (lower) undulator, respectively.

We call the 3rd term the spiral term. The spiral sense of rotation depends on the helicity of the undulator and the orientation is determined by the relative phase between the two light beams (constant phase term of the cos argument). The observation of the spiral term is an unambiguous proof for the presence of photons carrying OAM. The spiral term has a maximum if the argument of the cos function is zero which gives the correlation

$$\varphi = \pm \left(-\frac{\pi d}{\gamma^2 \lambda} + \frac{\pi d}{L^2 \lambda} r^2 \right) / (n - 1). \quad (5)$$

The term $(n - 1)$ represents the topological charge of the beam. A comparison of Eq. (5) with measurements permits the derivation of the sign and the absolute value of the topological charge from the sense of rotation and the shape of the spiral.

It must be emphasized that the electron beam emittance (i.e., transverse phase space volume) may have a significant impact on the OAM beam. Assuming the electron beam emittance being much larger than the OAM carrying photon beam of an individual electron, each electron still produces an OAM beam; however, the vortices of these

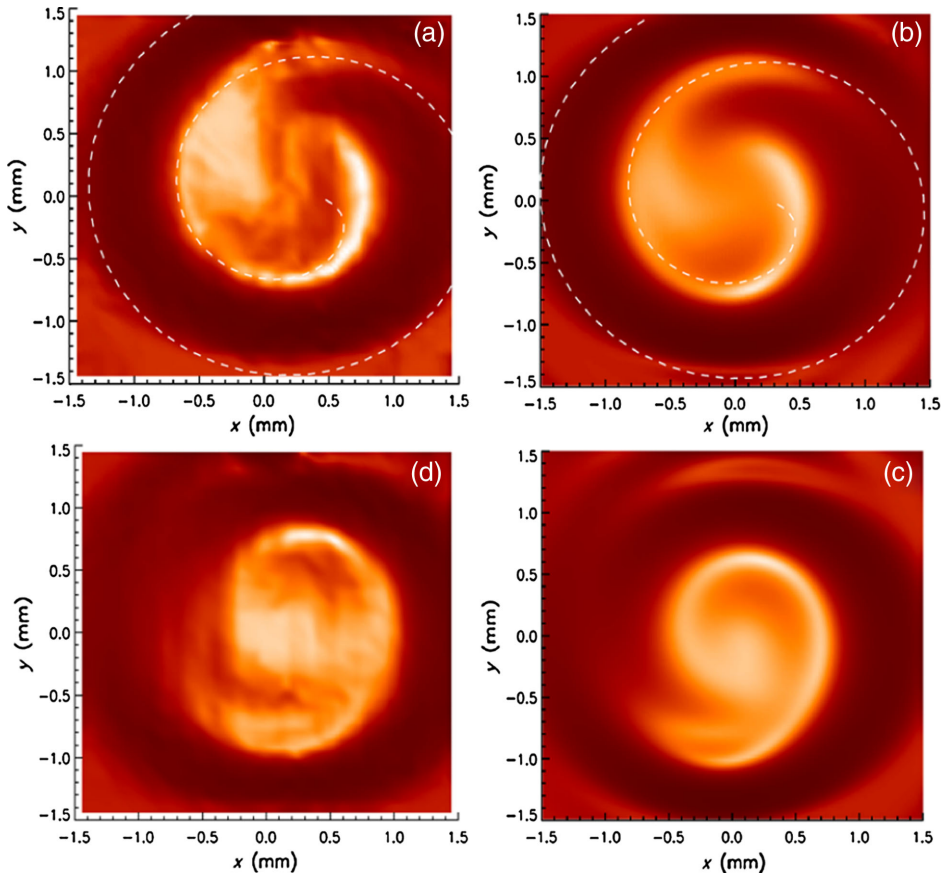


FIG. 4 (color online). Measurement [(a) and (d)] and simulation [(b) and (c)] for the case of 10° [(a) and (b)] and 0° [(d) and (c)] setting of the phase shifter. In the numeric simulations the spiral orientation is not a fitted parameter and the agreement with measurements demonstrates a realistic modeling of the undulators and the phase shifter. The dashed spirals in the upper plots are evaluated from the analytic equation Eq. (5) where the constant phase term is set to zero to match the observed orientation of the spiral.

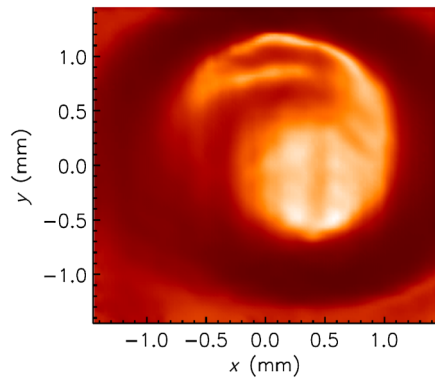


FIG. 5 (color online). Measured intensity distribution at 0° setting of the phase shifter and negative helicity. The spiral sense of rotation is reversed as compared to the results for positive helicity (Fig. 4).

individual beams are widely spread and the electron bunch does not produce a photon beam with a well-defined single vortex and a phase distribution as presented in [17].

The described interference experiment can only be performed with a sufficiently small electron beam emittance: Usually, BESSY II is operated at an electron energy of $E = 1.72$ GeV and a horizontal beam emittance of $\varepsilon_x = 6.20\pi \cdot \text{nm} \cdot \text{rad}$ (superconducting wavelength shifters switched off). The vertical emittance is a factor of 100 smaller (1% coupling ratio). These values have to be compared to the wavelength-dependent diffraction limited source size of the undulator radiation. Simulations with the synchrotron radiation code WAVE [24] demonstrate that the spiral intensity distribution is completely smeared out by the large horizontal emittance at $E = 1.72$ GeV. The horizontal emittance of a storage ring scales with the square of the electron energy [25]. To achieve the required degree of transverse coherence, the storage ring was ramped down with stored electron beam from $E = 1.72$ GeV to $E = 917$ MeV. The electron energy of this optics, which was established 10 years ago for the Physikalisch Technische Bundesanstalt, was determined earlier by means of Compton backscattering [26]. More recent measurements by one of the authors (P.S.) obtained a horizontal emittance of $\varepsilon_x = 1.66\pi \cdot \text{nm} \cdot \text{rad}$ and a natural fractional energy spread of $\sigma_E = 3.67 \times 10^{-4}$ for this setting. The typical beam current and lifetime during the measurements was 1 mA and 8 h, respectively.

Results.—The measured intensity distributions of the individual, noninterfering beams as emitted by the linear and helical undulator, respectively, are plotted in Fig. 3. As expected, the individual profiles do not show any spiral features. When overlapping the two beams coherently, a pronounced spiral intensity distribution becomes visible (Fig. 4). The spiral orientation depends on the angular settings of the phase shifter magnets and a rotation is visible when tuning the magnets from 0° to 10° . From magnetic measurements a path lengthening of 4.4 nm is expected for the 10° rotation. This corresponds to a relative

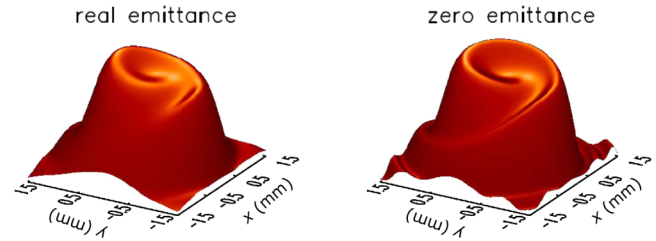


FIG. 6 (color online). 3D plots of simulations at 0° setting of the phase shifter and positive helicity of the upstream undulator [Fig. 4(c)] calculated for the actual (left) and zero (right) emittance, respectively.

phase change of 127° between the two undulator beams which is consistent with observation.

The measurements are reproduced by WAVE simulations utilizing realistic three-dimensional undulator and phase shifter fields. The excellent agreement between measurements and calculations validates the model underlying the simulations. The line of maximum intensity of the spiral structure is well reproduced by the analytical model of Eq. (5) [Fig. 4(a) and 4(b)].

Comparing Fig. 5 (negative helicity) and Fig. 4(a) (positive helicity) an opposite sense of rotation of the spiral intensity distributions for the two cases is observed. This is another proof of the existence of OAM photons. The spiral shape is slightly distorted for negative helicity due to electron beam steering caused by residual undulator field errors.

A comparison of simulations at zero and at actual emittance demonstrates, that even at $E = 917$ MeV the experimental results are still influenced by emittance effects (Fig. 6) due to lack of complete transversal coherence.

Under usual operation conditions of 3rd generation light sources with a typical emittance of $\varepsilon_x = 3\text{--}6\pi \cdot \text{nm} \cdot \text{rad}$ OAM carrying photon beams do not have a single, well-defined vortex with a distinct phase distribution of the wave front. Hence, they can hardly be observed utilizing interference methods. FEL arrangements for the production of x-ray photons carrying OAMs are complicated to be operated as pointed out earlier. This will be different for the next generation light sources currently under discussion: energy recovery linacs (ERLs) and ultimate storage rings (USRs), i.e., diffraction limited light sources. ERLs [27] are single (or few) turn storage rings which are filled with low emittance beams from a linac. The beam is extracted before being damped into an equilibrium state of larger emittance. USRs [28–31] on the other hand provide a low emittance even in the equilibrium.

Conclusion.—Our measurements clearly support predictions that the new accelerator-based diffraction limited light sources will deliver intense, clean, and energy-tunable OAM beams over a wide energy range with a single standard helical undulator under normal user conditions. The high energy limit of the extended photon beam parameter space is defined by the electron energy and the

emittance. It is expected that new exciting experiments with OAM carrying photon beams will become reality in many fields of research as soon as these radiation sources become operational.

The authors thank A. Gaupp, E. Gluskin, I. McNulty, and S. Sasaki for many helpful discussions.

-
- [1] L. Allen, M.W. Beijersbergen, R.J.C. Spreeuw, and J.P. Woerdman, *Phys. Rev. A* **45**, 8185 (1992).
- [2] M. Padgett, J. Courtial, and L. Allen, *Phys. Today* **57**, No. 5, 35 (2004).
- [3] *Twisted Photons, Application of Light with Orbital Angular Momentum*, edited by L. Torner and J. Torres (Wiley-VCH Verlag & Co. KGaH, Weinheim, Germany, 2011).
- [4] M. Padgett and R. Bowman, *Nat. Photonics* **5**, 343 (2011).
- [5] J. Wang *et al.*, *Nat. Photonics* **6**, 488 (2012).
- [6] M. van Veenendaal and I. McNulty, *Phys. Rev. Lett.* **98**, 157401 (2007).
- [7] S. Rehbein, P. Guttman, S. Werner, and G. Schneider, *Opt. Express* **20**, 5830 (2012).
- [8] S. Rehbein, S. Heim, P. Guttman, S. Werner, and G. Schneider, *Phys. Rev. Lett.* **103**, 110801 (2009).
- [9] M. Beijersbergen, L. Allen, H.E.L. O. van der Veen, and J.P. Woerdman, *Opt. Commun.* **96**, 123 (1993).
- [10] N.R. Heckenberg, R. McDuff, C.P. Smith, and A.G. White, *Opt. Lett.* **17**, 221 (1992).
- [11] A. Peele, K.A. Nugent, A.P. Mancuso, D. Paterson, I. McNulty, and J.P. Hayes, *J. Opt. Soc. Am. A* **21**, 1575 (2004).
- [12] Y. Kohmura, K. Sawada, M. Taguchi, T. Ishikawa, T. Ohigashi, and Y. Suzuki, *Appl. Phys. Lett.* **94**, 101112 (2009).
- [13] E. Hemsing, P. Musumeci, S. Reiche, R. Tikhoplav, A. Marinelli, J.B. Rosenzweig, and A. Gover, *Phys. Rev. Lett.* **102**, 174801 (2009).
- [14] E. Hemsing, A. Knyazik, F. O'Shea, A. Marinelli, P. Musumeci, O. Williams, S. Tochitsky, and J.B. Rosenzweig, *Appl. Phys. Lett.* **100**, 091110 (2012).
- [15] E. Hemsing, A. Marinelli, and J.B. Rosenzweig, *Phys. Rev. Lett.* **106**, 164803 (2011).
- [16] E. Hemsing and A. Marinelli, *Phys. Rev. Lett.* **109**, 224801 (2012).
- [17] S. Sasaki and I. McNulty, *Phys. Rev. Lett.* **100**, 124801 (2008).
- [18] S. Sasaki, I. McNulty, and R. Dejus, *Nucl. Instrum. Methods Phys. Res., Sect. A* **582**, 43 (2007).
- [19] J. Bahrtdt, W. Frentrup, A. Gaupp, M. Scheer, W. Gudat, G. Ingold, and S. Sasaki, *Nucl. Instrum. Methods Phys. Res., Sect. A* **467–468**, 21 (2001).
- [20] S. Sasaki, K. Kakuno, T. Takada, T. Shimada, K.-i. Yanagida, and Y. Miyahara, *Nucl. Instrum. Methods Phys. Res., Sect. A* **331**, 763 (1993).
- [21] M. Weiss *et al.*, *Nucl. Instrum. Methods Phys. Res., Sect. A* **467–468**, 449 (2001).
- [22] M.B. Moiseev, M.M. Nikitin, and N.I. Fedosov, *Sov. Phys. J.* **21**, 332 (1978).
- [23] K.-J. Kim, *Nucl. Instrum. Methods Phys. Res., Sect. B* **219**, 425 (1984).
- [24] M. Scheer, Ph.D. thesis, Humboldt University Berlin, Germany, vol. urn:nbn:de:kobv:11-10096299, 2008.
- [25] H. Wiedemann, *Particle Accelerator Physics I* (Springer-Verlag, Berlin, Heidelberg, New York, 2007), 3rd ed.
- [26] R. Klein, P. Kuske, R. Thornagel, G. Brandt, R. Görgen, and G. Ulm, *Nucl. Instrum. Methods Phys. Res., Sect. A* **486**, 545 (2002).
- [27] D. Bilderbeck, J.D. Brock, D.S. Dale, K.D. Finkelstein, M.A. Pfeifer, and S.M. Gruner, *New J. Phys.* **12**, 035011 (2010).
- [28] S.C. Leemann, Å. Andersson, M. Eriksson, L.-J. Lindgren, E. Wallén, J. Bengtsson, and A. Streun, *Phys. Rev. ST Accel. Beams* **12**, 120701 (2009).
- [29] L. Liu, N. Milas, A.H.C. Mukai, X.R. Resende, A.R.D. Rodrigues, and F.H. Sá, in *Proceedings of the International Particle Accelerator Conference (IPAC), Shanghai, China, 2013*, econf TUPWO001, 1874 (2013).
- [30] Y. Nosochkov, K.L.F. Bane, Y. Cai, R. Hettel, and M.-H. Wang, in *Proceedings of the International Particle Accelerator Conference (IPAC), San Sebastian, Spain, 2011*, econf THPC075, 3068 (2011).
- [31] M. Borland, in *Proceedings of the International Particle Accelerator Conference (IPAC), New Orleans, Louisiana, USA, 2012*, econf TUPPP033, 1683 (2012).